Non aligned hydrogen molecular ion in strong magnetic fields

D. Baye, A. Joos de ter Beerst‡ and J.-M. Sparenberg
Physique Quantique, C.P. 165/82,
Physique Nucléaire Théorique et Physique Mathématique, C.P. 229,
Université Libre de Bruxelles, B 1050 Brussels, Belgium

Abstract. The hydrogen molecular ion in a strong magnetic field is studied for arbitrary orientations of the molecular axis. A gauge preserving the parity symmetry and leading to real matrix elements for a class of basis states is introduced. The calculations are performed in prolate spheroidal coordinates with the Lagrange-mesh method. The simple resulting mesh equations provide a high accuracy with short computing times for $\gamma = 1$ and 10. Less accurate results are obtained at $\gamma = 100$ where the size of the matrix becomes very large. At such field strengths, the rotational motion becomes strongly hindered.

‡ Present address: *Centre de Recherche Astrophysique de Lyon (UMR CNRS 5574), Ecole Normale Supérieure de Lyon, 46 allée d'Italie, F-69364 Lyon cedex 07, France*

1. Introduction

Ultrastrong magnetic fields occur in the atmospheres of magnetic white dwarfs and neutron stars [1]. Unusual molecules that do not exist in the absence of magnetic fields may appear in this environment [2]. These molecules are usually studied with variational approximations whose accuracy is not well known. Since exotic molecules may be weakly bound, their very existence may be in question if calculations are not accurate enough. It is thus important to estimate the accuracy of variational calculations, and hence the validity of variational wave functions, on test cases. The simplest molecule, the hydrogen molecular ion H_2^+, allows studying its properties in strong magnetic fields with high accuracy. However, even for this simplest molecule, many questions still remain open.

Although purely quantal calculations are in principle possible, e.g. by combining the techniques described in [3, 4, 5, 6], their accuracy is still strongly restricted by computing time limitations. Studies based on the Born-Oppenheimer approximation, i.e. where the nuclei are fixed at some distance R, are thus still very useful (see [7, 8, 9, 10, 11, 12, 13, 14, 15, 16, 17] and references therein). The validity of that approximation has been discussed by Schmelcher *et al* [18].

In a first step, the molecular axis is usually aligned along the field axis. Different works have considered the more general non aligned case [7, 9, 11, 13].

Recently we have performed an accurate study of the aligned case [16]. To this end, we used the Lagrange-mesh method which is an approximate variational method simplified by the use of a consistent Gauss quadrature [19, 20, 21, 22, 23]. This method has provided accurate results for the hydrogen atom [24, 25] and the helium atom [6] in a magnetic field. The advantages of the Lagrange-mesh method are simplicity and accuracy. A high accuracy is obtained at the condition that the Hamiltonian does not possess any singularity or that singularities are regularized [21, 22, 23]. For H_2^+, the Coulomb singularities can be regularized in prolate spheroidal coordinates [16] (see also [26]). The aim of the present work is to extend the method to the non-aligned case and to provide highly accurate results under these assumptions at various field strengths. In order to keep the same basis and coordinate system as in [16], we fix the molecule axis and vary the field direction, contrary to most other works. We can then employ the same basis as in the aligned case but the magnetic quantum number is not any more a good quantum number.

In section 2, the Schrödinger equation for H_2^+ at the Born-Oppenheimer approximation is written for a magnetic field aligned in an arbitrary direction. The gauge choice is discussed. In section 3, the Lagrange-mesh method is applied in the system of prolate spheroidal coordinates. In section 4, accurate results are obtained at selected fields and angles. Energy surfaces are obtained and discussed. Concluding remarks are presented in section 5.

2. Gauge choice for arbitrary field directions

2.1. Schrödinger equation

The hydrogen molecular ion is treated at the Born-Oppenheimer approximation. Let R be the distance between the fixed protons, $\boldsymbol{r}_1$ and $\boldsymbol{r}_2$ the coordinates of the electron with respect to protons 1 and 2 and $\boldsymbol{r} = (x, y, z)$ the coordinate of the electron with respect to the centre of mass O of the protons.

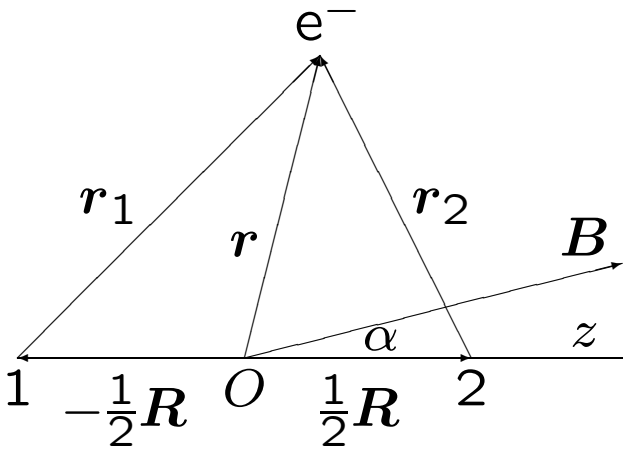

Figure 1. H_2^+ molecular ion at the Born-Oppenheimer approximation.

Contrary to other authors, we do not consider various directions of the molecule axis with respect to a fixed magnetic field $\boldsymbol{B}$ (see figure 1). In order to exploit a convenient coordinate system, we rather keep the molecule axis fixed and vary the field direction. In other words, the calculations are performed in the intrinsic reference frame of the molecule. This choice does not modify the values of energies. However wave functions at different angles are obtained in different reference frames. Using them in matrix elements requires performing a preliminary rotation in order to have a single direction for the field.

The Schrödinger equation for the hydrogen molecular ion in a magnetic field reads in atomic units

$$\left(\frac{1}{2}(\boldsymbol{p}+\boldsymbol{A})^2 + V(\boldsymbol{r})\right)\psi(\boldsymbol{r}) = E\psi(\boldsymbol{r}). \tag{1}$$

In this equation, $\boldsymbol{p}$ is the momentum of the electron and $\boldsymbol{A}$ is the vector potential defined in an arbitrary gauge by

$$\boldsymbol{B} = \nabla \times \boldsymbol{A}. \tag{2}$$

We choose $\nabla \cdot \boldsymbol{A} = 0$. The Coulomb interaction

$$V(\boldsymbol{r}) = \frac{1}{R} - \frac{1}{r_1} - \frac{1}{r_2} \tag{3}$$

possesses a cylindrical symmetry along the molecular axis.

2.2. Gauge choice

The probability density is symmetric with respect to the exchange of the protons. To prove this, we first choose a gauge for which the Hamiltonian is invariant under the parity operator Π with respect to the centre of mass of the protons,

$$\Pi H \Pi^\dagger = H. \tag{4}$$

Since the potential is invariant and $\boldsymbol{p}$ is a polar vector, $\boldsymbol{A}$ must be polar too,

$$\Pi \boldsymbol{A} \Pi^\dagger = -\boldsymbol{A}. \tag{5}$$

When (4) is satisfied, the eigenfunctions of H are either even or odd. Hence the probability density is even. Since the symmetric gauge

$$\boldsymbol{A}_S = \tfrac{1}{2}\boldsymbol{B} \times \boldsymbol{r} \tag{6}$$

has property (5), the probability density is symmetric with respect to proton exchange for that gauge choice. Therefore it must be symmetric for any gauge choice. This property is not always satisfied by approximate wave functions [13]. Property (5) is imposed to gauges in the following.

Let us now consider some general properties that can constrain the gauge to simplify the numerical calculations. In a variational study of equation (1), it is convenient to select a gauge for which the matrix elements are real. We assume that the basis states satisfy some rather general properties, i.e. that they are eigenstates of the parity operator

$$\Pi F_{ij}^{m\pi} = \pi F_{ij}^{m\pi} \tag{7}$$

and of the z component of the orbital momentum operator

$$L_z F_{ij}^{m\pi} = m F_{ij}^{m\pi}, \tag{8}$$

where i and j are some label indices (see equation (38)). We also assume that their phases satisfy

$$(F_{ij}^{m\pi})^* = F_{ij}^{-m\pi}. \tag{9}$$

Since the z-parity operator Π_z can be decomposed as

$$\Pi_z = \Pi e^{-i\pi L_z}, \tag{10}$$

the z-parity of the basis functions depends on m,

$$\pi_z = (-1)^m \pi. \tag{11}$$

Let us choose axis z along the molecule axis and axis y such that

$$\boldsymbol{B} \cdot \hat{\boldsymbol{y}} = 0. \tag{12}$$

The y-parity operator Π_y only changes the sign of the azimutal angle φ. Hence, with (9) and a relation similar to (10) along the y axis, the conjugate of a basis function is given by

$$(F_{ij}^{m\pi})^* = \Pi e^{-i\pi L_y} F_{ij}^{m\pi}. \tag{13}$$

Since $\boldsymbol{p}$ is imaginary, the conjugate of a matrix element can be written as

$$\begin{aligned}&\langle F_{ij}^{m\pi}|\tfrac{1}{2}(\boldsymbol{p}+\boldsymbol{A})^2+V(\boldsymbol{r})|F_{i'j'}^{m'\pi}\rangle^*\\&=\langle F_{ij}^{m\pi}|e^{i\pi L_y}[\tfrac{1}{2}(\boldsymbol{p}-\boldsymbol{A})^2+V(\boldsymbol{r})]e^{-i\pi L_y}|F_{i'j'}^{m'\pi}\rangle.\end{aligned}\tag{14}$$

Hence the matrix elements are real if $(\boldsymbol{p}-\boldsymbol{A})^2$ transforms into $(\boldsymbol{p}+\boldsymbol{A})^2$ under a rotation of angle π around the y axis, i.e. if $\boldsymbol{A}$ transforms as a pseudovector,

$$e^{i\pi L_y}(A_x,A_y,A_z)e^{-i\pi L_y}=(A_x,-A_y,A_z).\tag{15}$$

The most general divergenceless vector potential is

$$\boldsymbol{A}=\tfrac{1}{2}\boldsymbol{B}\times\boldsymbol{r}+\nabla F\tag{16}$$

with $\Delta F=0$. For simplicity, we restrict F to be quadratic in the coordinates. Then the most general function F satisfying (5) and (15) is

$$F=\tfrac{1}{2}(\lambda xy+\mu yz).\tag{17}$$

With this choice, parity is a good quantum number and matrix elements are real in a basis satisfying (7) to (9).

2.3. Prolate spheroidal coordinates

Equation (1) is best treated in the system of prolate spheroidal coordinates (ξ,η,φ) where φ is the azimutal angle and ξ and η are defined by

$$\xi=\frac{r_1+r_2}{R}-1\tag{18}$$

and

$$\eta=\frac{r_1-r_2}{R}.\tag{19}$$

Coordinate ξ is shifted with respect to traditional definitions in order that its definition interval be $(0,\infty)$. The volume element is given by

$$dV=\frac{1}{8}R^3J(\xi,\eta)d\xi d\eta d\varphi,\tag{20}$$

where the dimensionless part of the Jacobian reads

$$J(\xi,\eta)=(\xi+1)^2-\eta^2.\tag{21}$$

In this coordinate system, the Laplacian can be written as

$$\Delta=-\frac{4}{R^2J(\xi,\eta)}\,(T_\xi+T_\eta)+\frac{4}{R^2\xi(\xi+1)(1-\eta^2)}\frac{\partial^2}{\partial\varphi^2},\tag{22}$$

where the partial kinetic-energy operators are given by

$$T_\xi=-\frac{\partial}{\partial\xi}\xi(\xi+2)\frac{\partial}{\partial\xi}\tag{23}$$

and

$$T_\eta=-\frac{\partial}{\partial\eta}(1-\eta^2)\frac{\partial}{\partial\eta}.\tag{24}$$

The Coulomb potential becomes

$$V(\xi,\eta) = \frac{1}{R}\left(1 - \frac{4(\xi+1)}{(\xi+1)^2-\eta^2}\right). \tag{25}$$

The singularities of the potential and of the first term of the Laplacian are canceled in matrix elements by the $J(\xi,\eta)$ factor of the volume element. A singularity still occurs in the second term of the Laplacian.

2.4. Hamiltonian

With a field $\boldsymbol{B} = (B_x, 0, B_z)$ and gauge (16)-(17), the Hamiltonian takes the form

$$H = H_0 + H_1 + H_2 \tag{26}$$

with

$$H_0 = -\frac{1}{2}\Delta + V + \frac{1}{2}B_z L_z + \frac{1}{8}B_z^2(x^2+y^2) \tag{27}$$

i.e., H_0 is the Hamiltonian studied in [16], except for the replacement of B by B_z. The other terms read

$$H_1 = \frac{1}{2}\lambda y p_x + \frac{1}{2}[\lambda x + (\mu - B_x)z]p_y + \frac{1}{2}(\mu + B_x) y p_z \tag{28}$$

and

$$\begin{aligned} H_2 = \frac{1}{8}\Big\{&[\lambda(\lambda - 2B_z) + (\mu + B_x)^2]y^2 \\ &+[(\lambda + B_z)x + (\mu - B_x)z]^2 - B_z^2 x^2\Big\}. \end{aligned} \tag{29}$$

The simplest expression in prolate spheroidal coordinates is obtained with the choice $\lambda = 0$ and $\mu = B_x$, i.e.,

$$\boldsymbol{A} = (-\tfrac{1}{2}B_z y, \tfrac{1}{2}B_z x, B_x y). \tag{30}$$

The different terms become

$$H_0 = -\frac{1}{2}\Delta + V + \frac{1}{2}B_z L_z + \frac{R^2 B_z^2}{32}\xi(\xi+2)(1-\eta^2), \tag{31}$$

$$\begin{aligned} H_1 = &-iB_x \frac{[\xi(\xi+2)(1-\eta^2)]^{1/2}}{J(\xi,\eta)} \\ &\times \left[\xi(\xi+2)\eta\frac{\partial}{\partial\xi} + (\xi+1)(1-\eta^2)\frac{\partial}{\partial\eta}\right]\sin\varphi, \end{aligned} \tag{32}$$

and

$$H_2 = \frac{1}{8}R^2 B_x^2 \xi(\xi+2)(1-\eta^2)\sin^2\varphi. \tag{33}$$

The operators H_0, H_1 and H_2 correspond to $|\Delta m| = 0$, 1 and 2 couplings, respectively. The interest of the $\lambda = 0$ choice lies in the fact that $|\Delta m| = 2$ couplings do not occur because of H_1 and do thus not involve derivatives. With $\mu = B_x$, derivatives with respect to φ do not appear.

3. Lagrange-mesh method

3.1. Lagrange mesh and Lagrange basis

In order to solve equation (1), we introduce a Lagrange basis and the corresponding mesh [19, 20, 23].

The mesh contains $N_\xi N_\eta$ mesh points (hx_i, η_j) $(i = 1, \ldots, N_\xi,\ j = 1, \ldots, N_\eta)$. For each coordinate, the mesh points are defined in increasing order by

$$L_{N_\xi}(x_i) = 0 \tag{34}$$

and

$$P_{N_\eta}(\eta_j) = 0, \tag{35}$$

where L_n and P_n are Laguerre and Legendre polynomials, respectively [27]. The dimensionless parameter h allows scaling the Laguerre zeros in order to adapt the mesh to the size of the physical system. To each of these one-dimensional meshes is associated a Gauss quadrature formula

$$\int_0^\infty F(\xi)d\xi \approx h\sum_{i=1}^{N_\xi} \lambda_i F(hx_i) \tag{36}$$

and

$$\int_{-1}^{+1} G(\eta)d\eta \approx \sum_{j=1}^{N_\eta} \mu_j G(\eta_j), \tag{37}$$

where the λ_i and μ_j are the corresponding weights [27].

The infinitely differentiable three-dimensional basis functions are defined as the products

$$F_{ij}^{m\pi}(\xi, \eta, \varphi) = 2[\pi J_{ij} R^3]^{-1/2} f_i^{(\nu)}(\xi) g_{j\pi_z}^{(\nu)}(\eta) e^{im\varphi}, \tag{38}$$

where

$$J_{ij} = (hx_i + 1)^2 - \eta_j^2 \tag{39}$$

is the value of Jacobian (21) calculated at a mesh point, $\pi_z = \pm 1$ is the z-parity quantum number given by (11) and ν is a positive integer hereafter called 'regularization parameter'. Functions $f_i^{(\nu)}$ are regularized Lagrange-Laguerre functions [21, 22] defined as [16]

$$f_i^{(\nu)}(\xi) = (-1)^i (hx_i)^{1/2} \left(\frac{\xi(\xi+2)}{hx_i(hx_i+2)}\right)^{\frac{\nu}{2}} \frac{L_{N_\xi}(\xi/h)}{\xi - hx_i} e^{-\xi/2h}$$
$$i = 1, \ldots, \tfrac{1}{2}N_\xi. \tag{40}$$

The factor depending on ν may correct the behaviour of the Lagrange function at small ξ values. Similarly, assuming N_η even for simplicity, regularized Lagrange-Legendre functions are defined as [21]

$$g_{j\pi_z}^{(\nu)}(\eta) = \frac{1}{\sqrt{2}}[g_j^{(\nu)}(\eta) + \pi_z g_{N_\eta - j+1}^{(\nu)}(\eta)] \qquad j = 1, \ldots, \tfrac{1}{2}N_\eta, \tag{41}$$

where functions $g_j^{(\nu)}$ are defined as

$$g_j^{(\nu)}(\eta) = (-1)^{N_\eta - j}\sqrt{\frac{1-\eta_j^2}{2}}\left(\frac{1-\eta^2}{1-\eta_j^2}\right)^{\frac{\nu}{2}}\frac{P_{N_\eta}(\eta)}{\eta-\eta_j}. \tag{42}$$

Here the regularization factor modifies the Lagrange functions at ± 1. Together, the regularization factors in (40) and (42) compensate the singularity in the second term of Laplacian (22).

The one-dimensional Lagrange functions verify the simple properties

$$f_i^{(\nu)}(hx_{i'}) = (h\lambda_i)^{-1/2}\delta_{ii'} \tag{43}$$

and

$$g_{j\pi_z}^{(\nu)}(\eta_{j'}) = \mu_j^{-1/2}\delta_{jj'}. \tag{44}$$

These continuous functions vanish at all mesh points but one. Moreover they are orthonormal when overlaps are calculated with the appropriate Gauss quadrature [16]. This orthonormality may even be exact for low values of the regularization parameter ν. Hence the basis functions $F_{ij}^{m\pi}$ are also orthonormal when the integration over φ is performed analytically and the integrals over ξ and η are approximated with the Gauss quadrature.

3.2. Mesh equations

A wave function with parity π is expanded as

$$\psi^\pi(\xi,\eta,\varphi) = \sum_{m=m_{\min}}^{m_{\max}}\sum_{i=1}^{N_\xi}\sum_{j=1}^{\frac{1}{2}N_\eta} c_{ij}^{m\pi}F_{ij}^{m\pi}(\xi,\eta,\varphi) \tag{45}$$

where the $c_{ij}^{m\pi}$ are variational coefficients. When the integrals over ξ and η in the matrix elements are calculated with the Gauss-quadrature approximations (36) and (37), the variational equations take the form of mesh equations, similar to collocation equations.

The system of $\frac{1}{2}N_\xi N_\eta(m_{\max}-m_{\min}+1)$ Lagrange-mesh equations reads

$$\sum_{m'=m_{\min}}^{m_{\max}}\sum_{i'=1}^{N_\xi}\sum_{j'=1}^{N_\eta}(H_{ijm,i'j'm'}^{\pi} - E\delta_{ii'}\delta_{jj'}\delta_{mm'})c_{i'j'}^{m'\pi} = 0. \tag{46}$$

Because of the Gauss approximation, the matrix elements of the Hamiltonian are rather easy to establish and their computation is very fast. Different types of approximation are possible depending on the choice of the regularization power ν. As shown in [16], ν should be chosen even for even m values and odd for odd m values. For this reason, the square root in expression (32) of H_1 does not cause problems because all integrands encountered in the calculations are polynomials multiplied by the Laguerre weight $\exp(-\xi/h)$. Hence the Gauss quadrature is always a good approximation. Notice that as in other Lagrange-mesh calculations [22, 23], the accuracy on energies will be much better than the accuracy of the Gauss quadrature for individual matrix elements.

The expression of the H_0 part in (46) is given in [16], after multiplication by $\delta_{mm'}$. The expressions of the H_1 and H_2 parts are given in the appendix.

4. Results

The magnetic induction is expressed as $\gamma = B/B_0$ where $B_0 \approx 2.35 \times 10^5$ T. For the regularization parameter, we use $\nu = 0$ for $m = 0$, $\nu = 2$ for even m values and $\nu = 1$ for odd m values. These choices allow to better simulate the behaviour of the wave function in the vicinity of singular points. Selected eigenvalues of the large sparse symmetric matrix appearing in system (46) are searched for with the Jacobi-Davidson technique [28].

As usually in the Lagrange-mesh method, some parameters must be rather roughly optimized. The scaling parameter h is fixed at 0.2. Small variations around this value lead to insignificant modifications on the displayed energies. The numbers of mesh points N_ξ and N_η increase with the field strength. Equal or close values can be used for $\gamma = 1$ and 10 but N_η must be larger than N_ξ at higher fields. A new aspect here is that m is not a good quantum number for $\alpha \neq 0$. The bounds $m_{\min}$ and $m_{\max}$ in equation (45) vary with the angle. For small angles, the weak deviation with respect to the cylindrical symmetry allows rather small values of $|m_{\min}|$. The value of $m_{\max}$ may be smaller than $|m_{\min}|$ because positive m values have higher Landau thresholds and the contribution of the corresponding components is weaker. For angles close to 90°, a new symmetry imposes $m_{\max} = |m_{\min}|$. These values must thus be adapted to each angle.

Results for $\gamma = 1$ are given in Table 1. Here and below, all displayed digits are believed to be correct except the last one where an error of a few units is possible. Our energies are compared with the most accurate available results obtained by Larsen with the variational method and elaborate trial functions [17], for a fixed distance corresponding to the equilibrium distance at $\alpha = 0$. At this field, our results are significantly more accurate since we obtain about 10 significant digits. Larsen's results have an accuracy varying between 3×10^{-5} and 8×10^{-5} for α increasing from 15° to 90°. For each angle, the equilibrium distance varies. We also give their values in Table 1 together with the corresponding energies. The values 1.690 and 1.642 at 45° and 90° are slightly larger than those obtained in [13] by Turbiner and López Vieyra (1.667 and 1.635). The location of the energy minimum slightly decreases with increasing angle as expected from the fact that the magnetic field squeezes the electron wave function.

The corresponding energy surface is displayed as a function of R and α in figure 2. One observes that the valley is rather shallow and becomes narrower when α increases. Its shape does not vary much with the field angle except for the decrease of the minimum location already mentioned. The minimal energy progressively increases with angle α. Similar results can be found in Fig. 3 of [11].

Results for $\gamma = 10$ are displayed in Table 2. They are also compared with Larsen's variational results at $R = 0.958$. When the field strength increases, the number of stable digits decreases in the Lagrange-mesh method because of the increasing size of the matrix due to larger $m_{\max} - m_{\min}$. The physical eigenvalue corresponding to the ground state is not always the lowest one since the method is not purely variational

α (°)	$m_{\min}$	$m_{\max}$	R (a_0)	E (Hartree)	Ref. [17]
0	0	0	1.752	−0.474 988 244 647	
			1.75208	−0.474 988 245 274	
15	−12	6	1.752	−0.473 206 032 719	−0.473 17
			1.74268	−0.473 213 991 744	
30	−12	12	1.752	−0.468 385 599 03	−0.468 35
			1.71889	−0.468 490 782 84	
45	−20	12	1.752	−0.461 914 907 7	−0.461 86
			1.69015	−0.462 302 576 9	
60	−20	12	1.752	−0.455 574 447 6	−0.455 51
			1.66485	−0.456 380 746 1	
75	−20	16	1.752	−0.451 014 467 6	−0.450 94
			1.64810	−0.452 195 150 3	
90	−20	20	1.752	−0.449 362 477 9	
			1.64229	−0.450 692 199 5	

Table 1. Energies E at $\gamma = 1$ and $R = 1.752$ compared with the results of Larsen [17] as a function of angle α (upper line). Equilibrium distances R_e and energies E (lower line). Calculations are performed with $N_\xi = N_\eta = 20$ and $h = 0.2$.

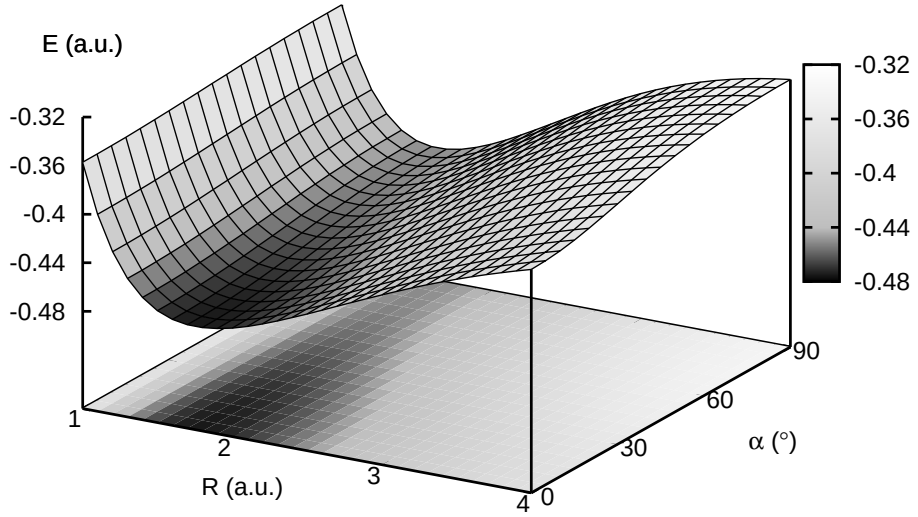

Figure 2. Ground-state energy surface of H_2^+ at $\gamma = 1$ as a function of the interproton distance R and of the field angle α.

because of the Gauss quadrature. The ground-state eigenvalue can be identified because its digits are stable. At this field, we obtain about 7 significant digits. Larsen's results have an accuracy varying between 1.5×10^{-4} and 6×10^{-4} for α increasing from 15° to 90°. We also give for each angle in Table 2 an accurate equilibrium distance and the corresponding energy. The values 0.834 and 0.780 at 45° and 90° are also slightly larger

α (°)	$m_{\min}$	$m_{\max}$	R (a_0)	E (Hartree)	Ref. [17]
0	0	0	0.958	2.825 014 661	
			0.95702	2.825 013 965	
15	−20	8	0.958	2.851 849 78	2.852 02
			0.93117	2.851 280 65	
30	−24	8	0.958	2.920 713 3	2.921 00
			0.87981	2.915 153 5	
45	−36	8	0.958	3.004 869 7	3.005 24
			0.83394	2.989 554 8	
60	−46	12	0.958	3.078 507 9	3.078 95
			0.80260	3.053 937 8	
75	−40	18	0.958	3.126 301 8	3.126 86
			0.78527	3.096 388 6	
90	−30	30	0.958	3.142 585 8	
			0.77982	3.111 105 1	

Table 2. Energies E at $\gamma = 10$ and $R = 0.958$ compared with the results of Larsen [17] as a function of angle α (upper line). Equilibrium distances R_e and energies E (lower line). Calculations are performed with $N_\xi = 24$, $N_\eta = 28$ and $h = 0.2$.

than those obtained by Turbiner and López Vieyra (0.812 and 0.772).

The energy surface at $\gamma = 10$ is presented in figure 3. With respect to $\gamma = 1$, the valley is narrower and displays a steeper increase of the minimum. Its shape varies more with the field angle.

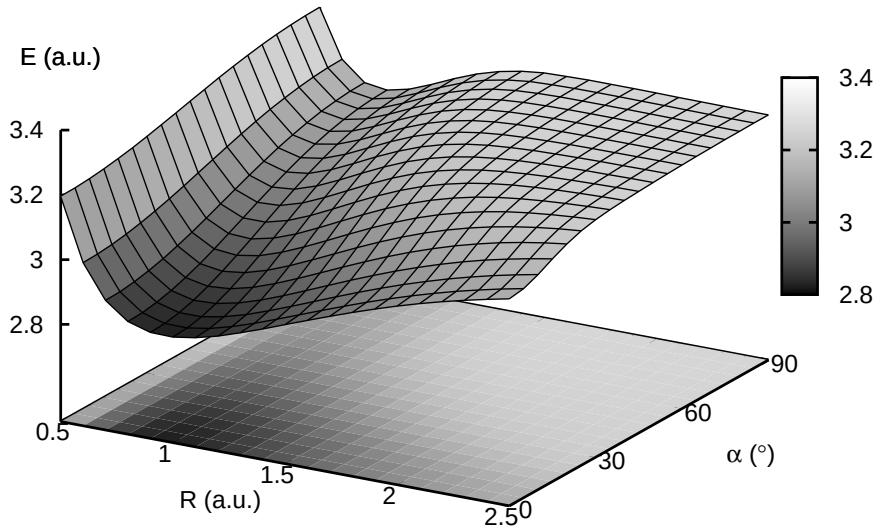

Figure 3. Ground-state energy surface of H_2^+ at $\gamma = 10$ as a function of the interproton distance R and of the field angle α.

For $\gamma = 100$, the situation is more difficult. The size of the matrix becomes very large. The worst difficulty is due to the occurrence of many unphysical eigenvalues below and around the physical eigenvalue corresponding to the ground state. When convergence is good enough, the ground-state energy can anyway be identified among the other ones by its stability. Results displaying the significant digits are presented in Table 3. They are obtained with $N_\eta \approx 2N_\xi$. Since the size of the matrix increases with angle α, only the first values of this angle could be accurately studied. Beyond 15°, fewer digits are stable. Our results still improve those of Larsen by about 3×10^{-3} to 6×10^{-3}. An accurate equilibrium distance and the corresponding energy are also given in Table 3. The values 0.346 and 0.336 at 45° and 90° are also slightly larger than the values 0.337 and 0.320 obtained in [13].

α (°)	$m_{\min}$	$m_{\max}$	R (a_0)	E (Hartree)	Ref. [17]
0	0	0	0.448	44.853 918 878	
			0.44779	44.853 918 538	
15	−28	8	0.448	45.043 794	45.046 6
			0.4174	45.034 863	
30	−40	8	0.448	45.477 1	45.480 8
			0.3747	45.416 0	
45	−62	8	0.448	45.906 1	45.909 3
			0.346	45.800 7	
60	−68	10	0.448	46.191 9	46.196 1
			0.336	46.099 0	
75	−68	20	0.448	46.333 4	46.340 0
			0.335	46.280 0	
90	−48	48	0.448	46.374 4	
			0.336	46.339 7	

Table 3. Energies E at $\gamma = 100$ and $R = 0.448$ compared with the results of Larsen [17] as a function of angle α (upper line). Equilibrium distances R_e and energies E (lower line). Calculations are performed with $N_\xi = 20$ or 24, $N_\eta = 40$ or 44 and $h = 0.2$.

The energy surface at $\gamma = 100$ is presented in figure 4. It is completely different from the $\gamma = 1$ case. The valley is now aligned along the field axis. The rotation of the molecular axis is almost totally hindered.

The behaviour with respect to rotations has been parametrized by Larsen as [7, 17]

$$E(R_e, \alpha) = E(R_e, 0) + A_{R_e} \sin^2 \alpha. \tag{47}$$

Values for A_{R_e} are given in Table 4. They are very close to those of Larsen [17]. The agreement improves with increasing field strength. The limit $\alpha_{1\%}$ of the domain where this approximation is valid within 1 % is also displayed. Approximation (47) is particularly good at $\gamma = 1$ where its accuracy is still better than 2 % at $\alpha = 45°$.

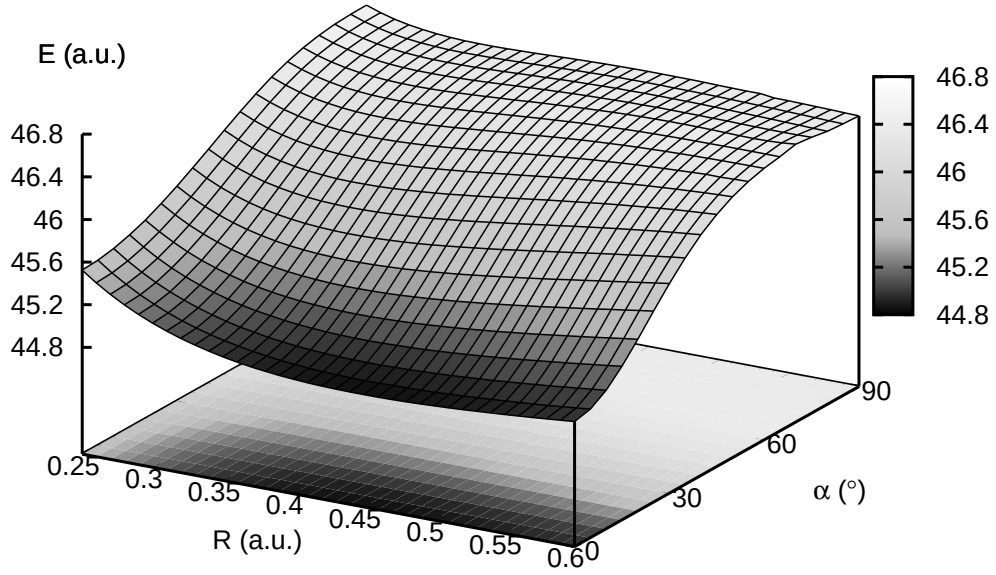

Figure 4. Ground-state energy surface of H_2^+ at $\gamma = 100$ as a function of the interproton distance R and of the field angle α.

γ	R_e	A_{R_e}	$\alpha_{1\%}$ (°)	A_{R_e} [17]
1	1.75208	0.026 679	30	0.0285
10	0.95702	0.406 70	11	0.409
100	0.44779	2.969	7	2.96

Table 4. Equilibrium distances R_e and coefficients A_{R_e} of approximation (47) as a function of γ, compared with the results of Larsen [17].

5. Conclusions

The hydrogen molecular ion in a strong magnetic field has been studied for arbitrary orientations of the molecular axis. Rather than rotating the molecule axis, we change the field direction to allow the use of the same prolate spheroidal coordinates at each angle. A coupling then appears between different magnetic quantum numbers which strongly increases the basis size.

The Lagrange-mesh method simplifies the calculation while allowing to obtain highly accurate results. To simplify its use, we have introduced a gauge leading to the simplest forms for the couplings between different m values. For the field strengths $\gamma = 1$ and $\gamma = 10$, we obtain very accurate results with short computing times. At $\gamma = 100$ and higher fields, the size of the matrix becomes very large and the occurrence of unphysical eigenvalues due to the Gauss approximation inherent in the Lagrange-mesh method makes the search for physical eigenvalues much more tedious.

Energy surfaces display the progressive disparition of the rotation degree of freedom of the molecule with increasing magnetic fields. From $\gamma = 1$ to $\gamma = 100$, the valley of local minima of the energy rotates. It evolves from a rather weak angular dependence to

an alignment along the field axis. At $\gamma = 100$, the rotational motion is already strongly hindered. The aligned approximation should be quite valid beyond that field.

Acknowledgments

This text presents research results of the Belgian program P6/23 on interuniversity attraction poles initiated by the Belgian Federal Science Policy Office.

Appendix A. Matrix elements of H_1 and H_2

The matrix elements of H_0 are given in [16]. Different options are available: symmetrized (equations (41) to (45)) or integrated by parts (equations (46) to (51)). Here we give the matrix elements of H_1 and H_2.

Let us start with the first term of equation (32), i.e. the term containing the derivative with respect to ξ, hereafter called H_{1a}. By using the Gauss quadrature and the expresssions

$$f_{i'}^{(\nu)\prime}(hx_i) = (h\lambda_{i'})^{-1/2}\frac{(-1)^{i-i'}}{h(x_i-x_{i'})}\sqrt{\frac{x_{i'}}{x_i}}\left[\frac{x_i(hx_i+2)}{x_{i'}(hx_{i'}+2)}\right]^{\nu/2} \tag{A.1}$$

for $i \neq i'$ and

$$f_{i}^{(\nu)\prime}(hx_i) = (h\lambda_{i})^{-1/2}\frac{1}{2hx_i}\left(2\nu - 1 - \frac{2\nu}{hx_i+2}\right), \tag{A.2}$$

one obtains for $i \neq i'$

$$\begin{aligned}\langle F_{ij}^{m\pi}|H_{1a}|F_{i'j'}^{m'\pi}\rangle = & -\frac{1}{2}(\delta_{m,m'-1}-\delta_{m,m'+1})\eta_j\sqrt{1-\eta_j^2}\delta_{jj'}(J_{ij}J_{i'j})^{-1/2} \\ & \times\frac{(-1)^{i-i'}}{h(x_i-x_{i'})}\sqrt{\frac{x_{i'}}{x_i}}\frac{[hx_i(hx_i+2)]^{(\nu'+3)/2}}{[hx_{i'}(hx_{i'}+2)]^{\nu'/2}}\end{aligned} \tag{A.3}$$

and for $i = i'$

$$\begin{aligned}\langle F_{ij}^{m\pi}|H_{1a}|F_{ij'}^{m'\pi}\rangle = & -\frac{1}{2}(\delta_{m,m'-1}-\delta_{m,m'+1})\eta_j\sqrt{1-\eta_j^2}\delta_{jj'}J_{ij}^{-1} \\ & \times\left[(\nu'-\tfrac{1}{2})(hx_i+2)-\nu'\right][hx_i(hx_i+2)]^{1/2}.\end{aligned} \tag{A.4}$$

Let us turn to the second term H_{1b} of equation (32), i.e. the term containing the derivative with respect to η. By using the Gauss quadrature and the expresssions

$$g_{j'}^{(\nu)\prime}(\eta_j) = \mu_{j'}^{-1/2}\frac{(-1)^{j-j'}}{\eta_j-\eta_{j'}}\left(\frac{1-\eta_j^2}{1-\eta_{j'}^2}\right)^{(\nu-1)/2} \tag{A.5}$$

for $j \neq j'$ and

$$g_{j}^{(\nu)\prime}(\eta_j) = \mu_{j}^{-1/2}(1-\nu)\frac{\eta_j}{1-\eta_j^2}, \tag{A.6}$$

one obtains for $j \neq j'$

$$\langle F_{ij}^{m\pi}|H_{1b}|F_{i'j'}^{m'\pi}\rangle = -\frac{1}{2}(\delta_{m,m'-1}-\delta_{m,m'+1})(hx_i+1)[hx_i(hx_i+2)]^{1/2}$$

$$\times \delta_{ii'}(J_{ij}J_{ij'})^{-1/2}(-1)^{j-j'}\left(\frac{1}{\eta_j-\eta_{j'}}-\frac{\pi_z}{\eta_j+\eta_{j'}}\right)$$
$$\times \frac{(1-\eta_j^2)^{(\nu'+2)/2}}{(1-\eta_{j'}^2)^{(\nu'-1)/2}} \qquad (A.7)$$

and for $j=j'$

$$\langle F_{ij}^{m\pi}|H_{1b}|F_{i'j}^{m'\pi}\rangle = -\frac{1}{2}(\delta_{m,m'-1}-\delta_{m,m'+1})(hx_i+1)[hx_i(hx_i+2)]^{1/2}$$
$$\times \delta_{ii'}J_{ij}^{-1}\left[(1-\nu')\eta_j-\pi_z\frac{1-\eta_j^2}{2\eta_j}\right](1-\eta_j^2)^{1/2}. \qquad (A.8)$$

Now we can calculate the matrix elements of $H_1=H_{1a}+H_{1b}$. The expressions we have obtained are however not symmetrical with respect to transposition, i.e. the matrix element and its transposed are not equal at the Gauss approximation. This drawback is solved by applying the Gauss approximation to the average of each matrix element and of its transposed. In other words, we have to symmetrize expressions (A.3), (A.7) and the sum of (A.4) and (A.8).

For $i\neq i'$, only the ξ-dependent part is modified and the matrix element (A.3) provides

$$\langle F_{ij}^{m\pi}|H_1|F_{i'j'}^{m'\pi}\rangle = -\frac{1}{4}(\delta_{m,m'-1}-\delta_{m,m'+1})\eta_j\sqrt{1-\eta_j^2}\delta_{jj'}(J_{ij}J_{i'j})^{-1/2}$$
$$\times \frac{(-1)^{i-i'}}{h(x_i-x_{i'})}\left\{\sqrt{\frac{x_{i'}}{x_i}}\frac{[hx_i(hx_i+2)]^{(\nu'+3)/2}}{[hx_{i'}(hx_{i'}+2)]^{\nu'/2}}\right.$$
$$\left.+\sqrt{\frac{x_i}{x_{i'}}}\frac{[hx_{i'}(hx_{i'}+2)]^{(\nu+3)/2}}{[hx_i(hx_i+2)]^{\nu/2}}\right\}. \qquad (A.9)$$

For $j\neq j'$, only the η-dependent part is modified and the matrix element (A.7) provides

$$\langle F_{ij}^{m\pi}|H_1|F_{i'j'}^{m'\pi}\rangle = -\frac{1}{4}(\delta_{m,m'-1}-\delta_{m,m'+1})(hx_i+1)[hx_i(hx_i+2)]^{1/2}$$
$$\times \delta_{ii'}(J_{ij}J_{ij'})^{-1/2}(-1)^{j-j'}\left(\frac{1}{\eta_j-\eta_{j'}}-\frac{\pi_z}{\eta_j+\eta_{j'}}\right)$$
$$\times \left[\frac{(1-\eta_j^2)^{(\nu'+2)/2}}{(1-\eta_{j'}^2)^{(\nu'-1)/2}}+\frac{(1-\eta_{j'}^2)^{(\nu+2)/2}}{(1-\eta_j^2)^{(\nu-1)/2}}\right]. \qquad (A.10)$$

For $i=i'$ and $j=j'$, the symmetrized sum of (A.4) and (A.8) is

$$\langle F_{ij}^{m\pi}|H_1|F_{ij}^{m'\pi}\rangle = \frac{1}{4}(\delta_{m,m'-1}-\delta_{m,m'+1})(hx_i+1)[hx_i(hx_i+2)]^{1/2}$$
$$\times \delta_{ii'}J_{ij}^{-1}\pi_z\eta_j^{-1}(1-\eta_j^2)^{3/2}. \qquad (A.11)$$

Though heavy, expressions (A.9) and (A.10) are easily programmed and are computed in a very short time.

The matrix elements of H_2 are very simple,

$$\langle F_{ij}^{m\pi}|H_2|F_{ij'}^{m'\pi}\rangle = \frac{R^2B_x^2}{32}(2\delta_{mm'}-\delta_{m,m'-2}-\delta_{m,m'+2})$$
$$\times hx_i(hx_i+2)(1-\eta_j^2)\delta_{ii'}\delta_{jj'}. \qquad (A.12)$$

The $|\Delta m|=2$ blocks are diagonal.

References

[1] Lai D 2001 *Rev. Mod. Phys.* **73** 629-62
[2] Turbiner A V and López Vieyra J C 2006 *Phys. Rep.* **424** 309-96
[3] Hesse M and Baye D 1999 *J. Phys. B: At. Mol. Opt. Phys.* **32** 5605-17
[4] Hesse M and Baye D 2001 *J. Phys. B: At. Mol. Opt. Phys.* **34** 1425-42
[5] Hesse M and Baye D 2003 *J. Phys. B: At. Mol. Opt. Phys.* **36** 139-54
[6] Hesse M and Baye D 2004 *J. Phys. B: At. Mol. Opt. Phys.* **37** 3937-46
[7] Larsen D M 1982 *Phys. Rev.* A **25** 1295-304
[8] Vincke M and Baye D 1985 *J. Phys. B: At. Mol. Opt. Phys.* **18** 167-76
[9] Wille U 1988 *Phys. Rev.* A **38** 3210-35
[10] Kappes U and Schmelcher P 1995 *Phys. Rev.* A **51** 4542-57
[11] Kappes U and Schmelcher P 1996 *Phys. Rev.* A **53** 3869-83
[12] Kravchenko Y P and Liberman M A 1997 *Phys. Rev.* A **55** 2701-10
[13] Turbiner A V and López Vieyra J C 2003 *Phys. Rev.* A **68** 012504
[14] Guan X, Li B and Taylor K T 2003 *J. Phys. B: At. Mol. Opt. Phys.* **36** 3569-90
[15] Turbiner A V and López Vieyra J C 2004 *Phys. Rev.* A **69** 053413
[16] Vincke M and Baye D 2006 *J. Phys. B: At. Mol. Opt. Phys.* **39** 2605-18
[17] Larsen D M 2007 *Phys. Rev.* A **76** 042502
[18] Schmelcher P, Cederbaum L S and Meyer H-D 1988 *Phys. Rev.* A **38** 6066-79
[19] Baye D and Heenen P-H 1986 *J. Phys. A: Math. Gen.* **19** 2041-59
[20] Baye D and Vincke M 1991 *J. Phys. B: At. Mol. Opt. Phys.* **24** 3551-64
[21] Vincke M, Malegat L and Baye D 1993 *J. Phys. B: At. Mol. Opt. Phys.* **26** 811-26
[22] Baye D, Hesse M and Vincke M 2002 *Phys. Rev.* E **65** 026701
[23] Baye D 2006 *Phys. Stat. Sol.* (b) **243** 1095-109
[24] Baye D, Vincke M and Hesse M 2008 *J. Phys. B: At. Mol. Opt. Phys.* **41** 055005
[25] Baye D, Hesse M and Vincke M 2008 *J. Phys. B: At. Mol. Opt. Phys.* **41** 185002
[26] Tao L, McCurdy C W and Rescigno T N 2009 *Phys. Rev.* A **79** 012719
[27] Abramowitz M and Stegun I A 1965 *Handbook of Mathematical Functions* (New York: Dover)
[28] Bollhöfer M and Notay Y 2007 *Comp. Phys. Comm.* **177** 951-64; available via http://homepages.ulb.ac.be/∼jadamilu/